Supplemental figures and legends

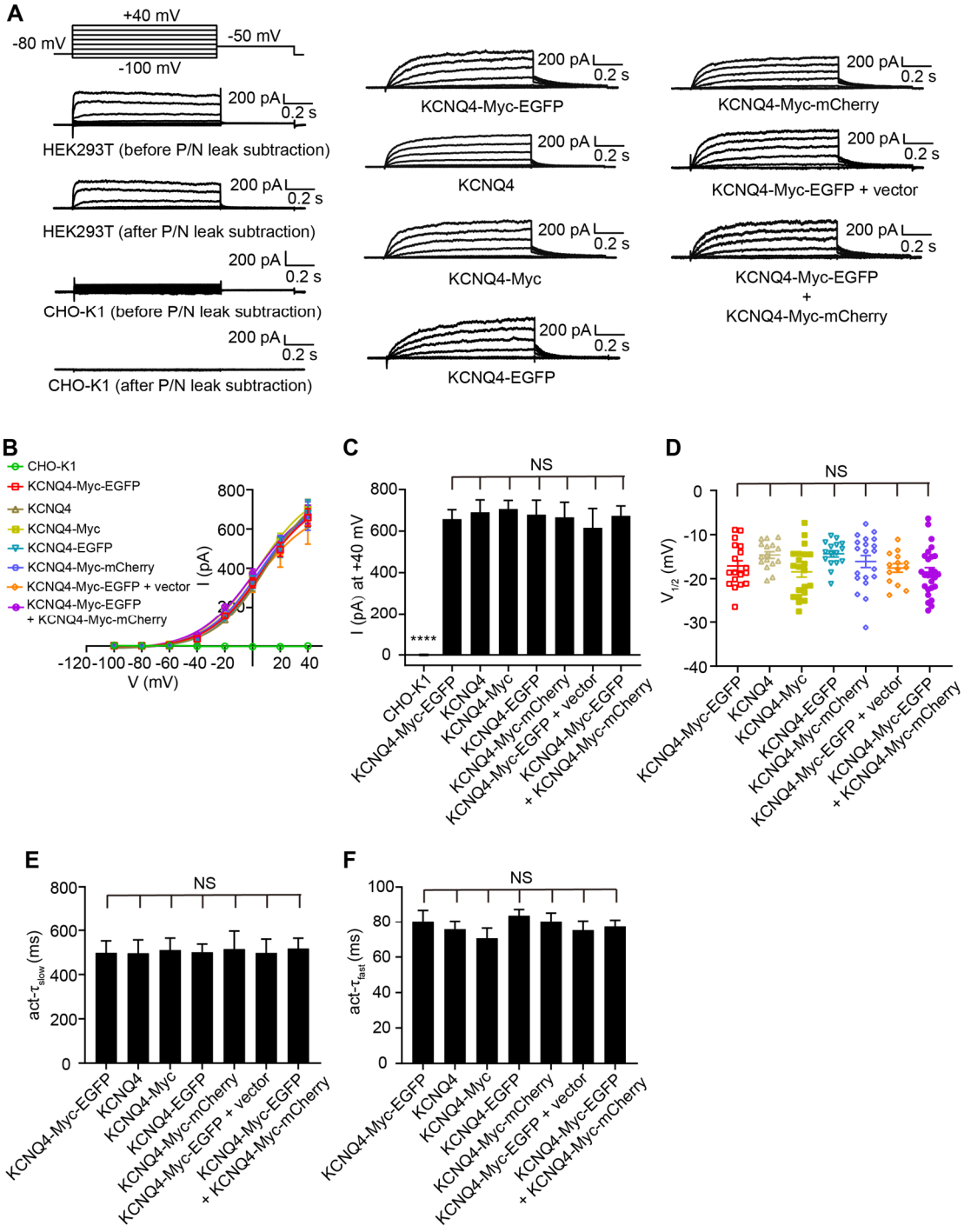

Supplemental Fig. S1: Whole-cell currents of wild-type KCNQ4. (A) Representative current traces of un-transfected HEK293T (before and after P/N leak subtraction), un-transfected CHO-K1 (before and after P/N leak subtraction), KCNQ4-Myc-EGFP, KCNQ4, KCNQ4-Myc, KCNQ4-EGFP, KCNQ4-Myc-mCherry, KCNQ4-

Myc-EGFP + vector (1:1), and KCNQ4-Myc-EGFP + KCNQ4-Myc-mCherry (1:1). Cells were held at -80 mV. Step voltages ranged from -100 to +40 mV with 20 mV increments, followed by a pulse of -50 mV. (B) Mean current-voltage relation of un-transfected CHO-K1, KCNQ4-Myc-EGFP, KCNQ4, KCNQ4-Myc, KCNQ4-EGFP, KCNQ4-Myc-mCherry, KCNQ4-Myc-EGFP + vector (1:1), and KCNQ4-Myc-EGFP + KCNQ4-Myc-mCherry (1:1) (n = 18, 24, 28, 20, 19, 26, 16, 40; mean ± SEM). (C) Summary bar graph of steady-state currents elicited at +40 mV, obtained from whole-cell current recordings as presented in (A). Average whole-cell currents (pA) at +40 mV were 0.12 ± 2.33, 657.82 ± 45.57, 690.80 ± 59.18, 706.39 ± 40.91, 679.22 ± 69.51, 665.83 ± 72.75, 615.31 ± 93.13, and 673.2 ± 48.03 for CHO-K1, KCNQ4-Myc-EGFP, KCNQ4, KCNQ4-Myc, KCNQ4-EGFP, KCNQ4-Myc-mCherry, KCNQ4-Myc-EGFP + vector (1:1), and KCNQ4-Myc-EGFP + KCNQ4-Myc-mCherry (1:1), respectively. (D) Individual $V_{1/2}$ values for KCNQ4-Myc-EGFP, KCNQ4, KCNQ4-Myc, KCNQ4-EGFP, KCNQ4-Myc-mCherry, KCNQ4-Myc-EGFP + vector (1:1), and KCNQ4-Myc-EGFP + KCNQ4-Myc-mCherry (1:1). (E) Data for the average time constants at +40 mV of the slow activation component. (F) Data for the average time constants at +40 mV of the fast activation component. Data represent the mean ± SEM. Statistical analysis was performed using one-way ANOVA with Dunnett analysis. ****$P < 0.0001$. NS indicates no significant difference, compared to KCNQ4-Myc-EGFP.

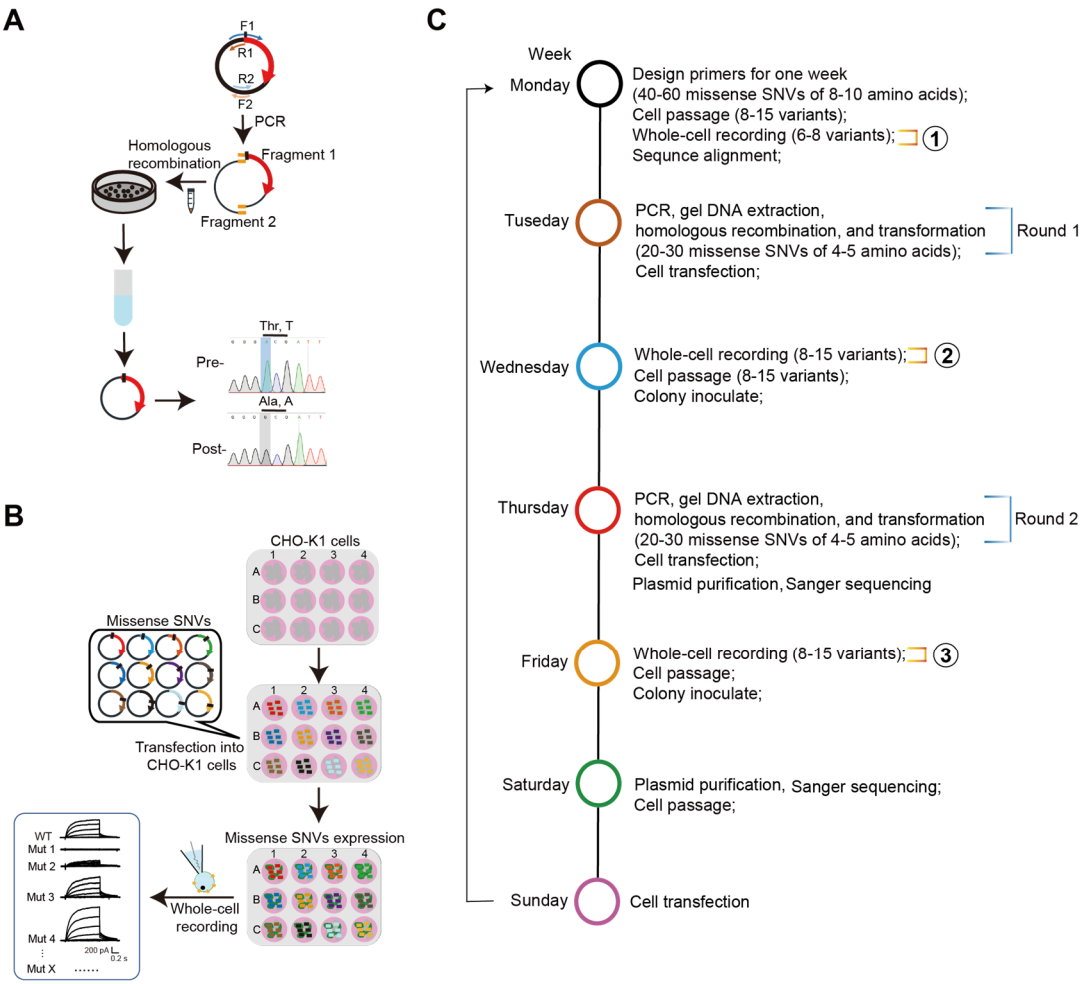

Supplemental Fig. S2: Workflow for *KCNQ4* variants generation and functional testing. (A) Overall scheme for generation of *KCNQ4* variants. (B) Overview of variant functional testing via patch-clamp recording. (C) An example of schedule for variant plasmid construction and patch-clamp recording for one week.

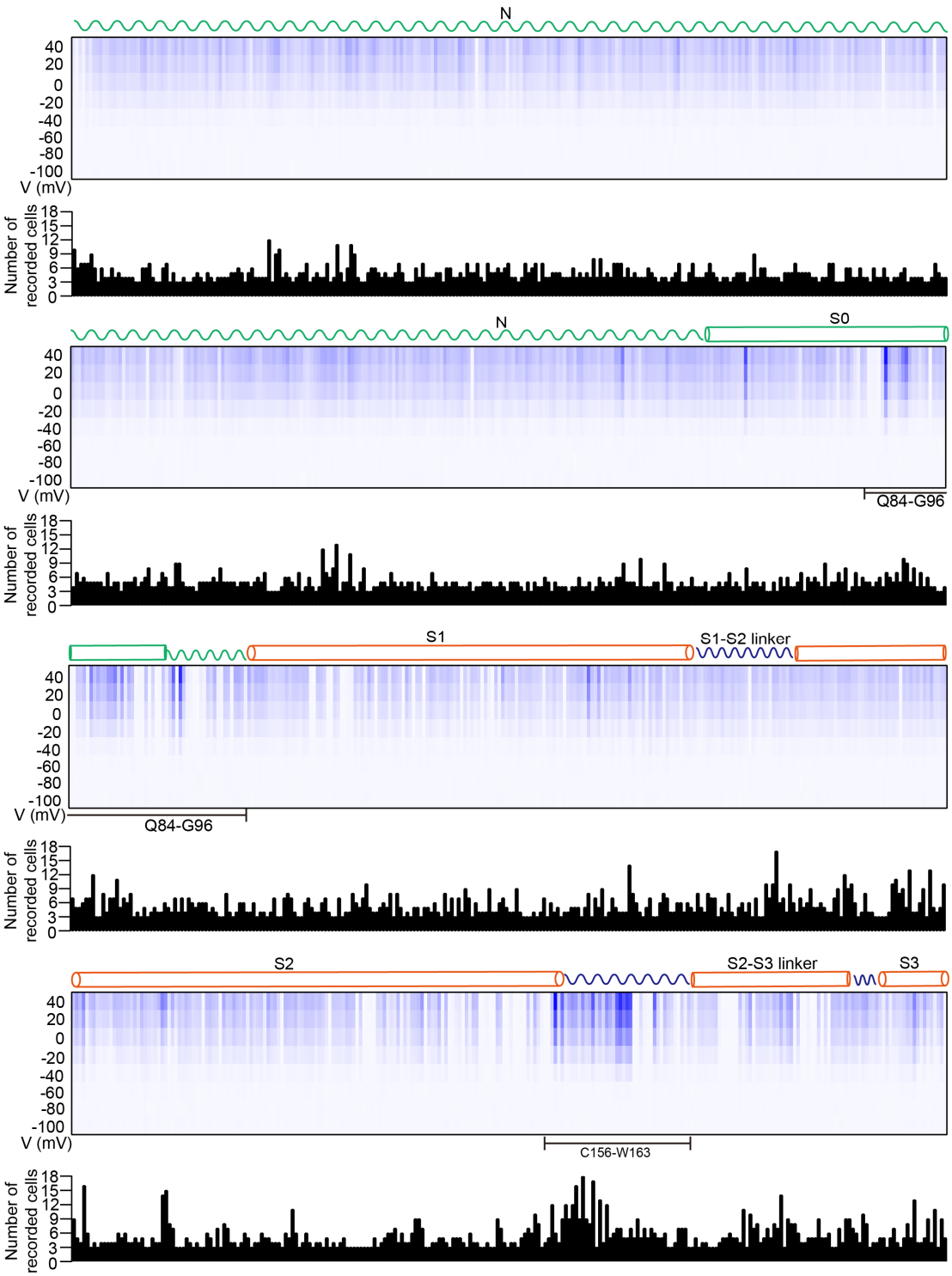
N
40
20
0
-20
-40
-60
-80
-100
V (mV)
Number of recorded cells
18
15
12
9
6
3
0
N
S0
Q84-G96
S1
S1-S2 linker
Q84-G96
S2
S2-S3 linker
S3
C156-W163

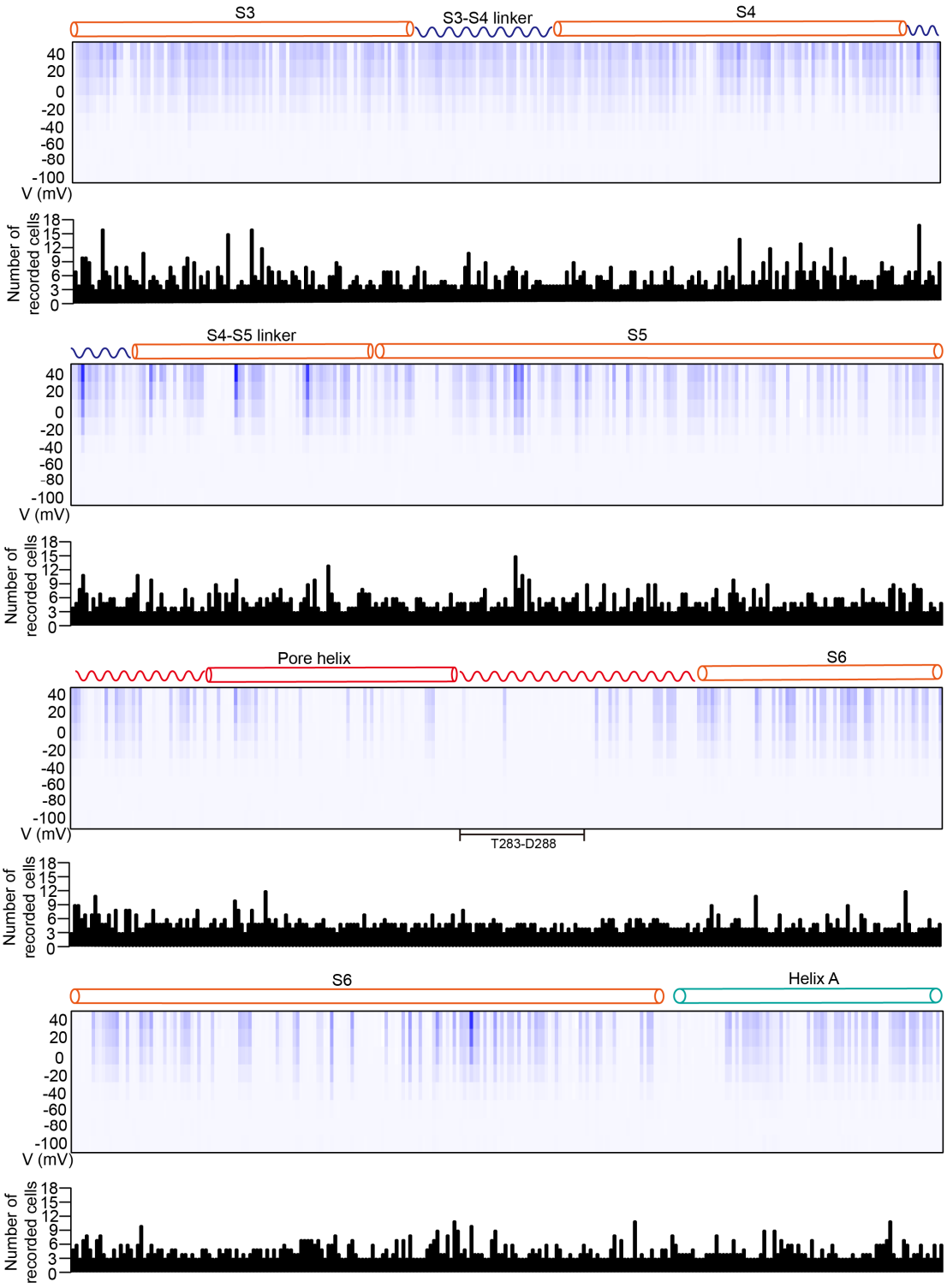
S3
S3-S4 linker
S4
40
20
0
-20
-40
-60
-80
-100
V (mV)
Number of recorded cells
18
15
12
9
6
3
0
S4-S5 linker
S5
Pore helix
S6
T283-D288
Helix A

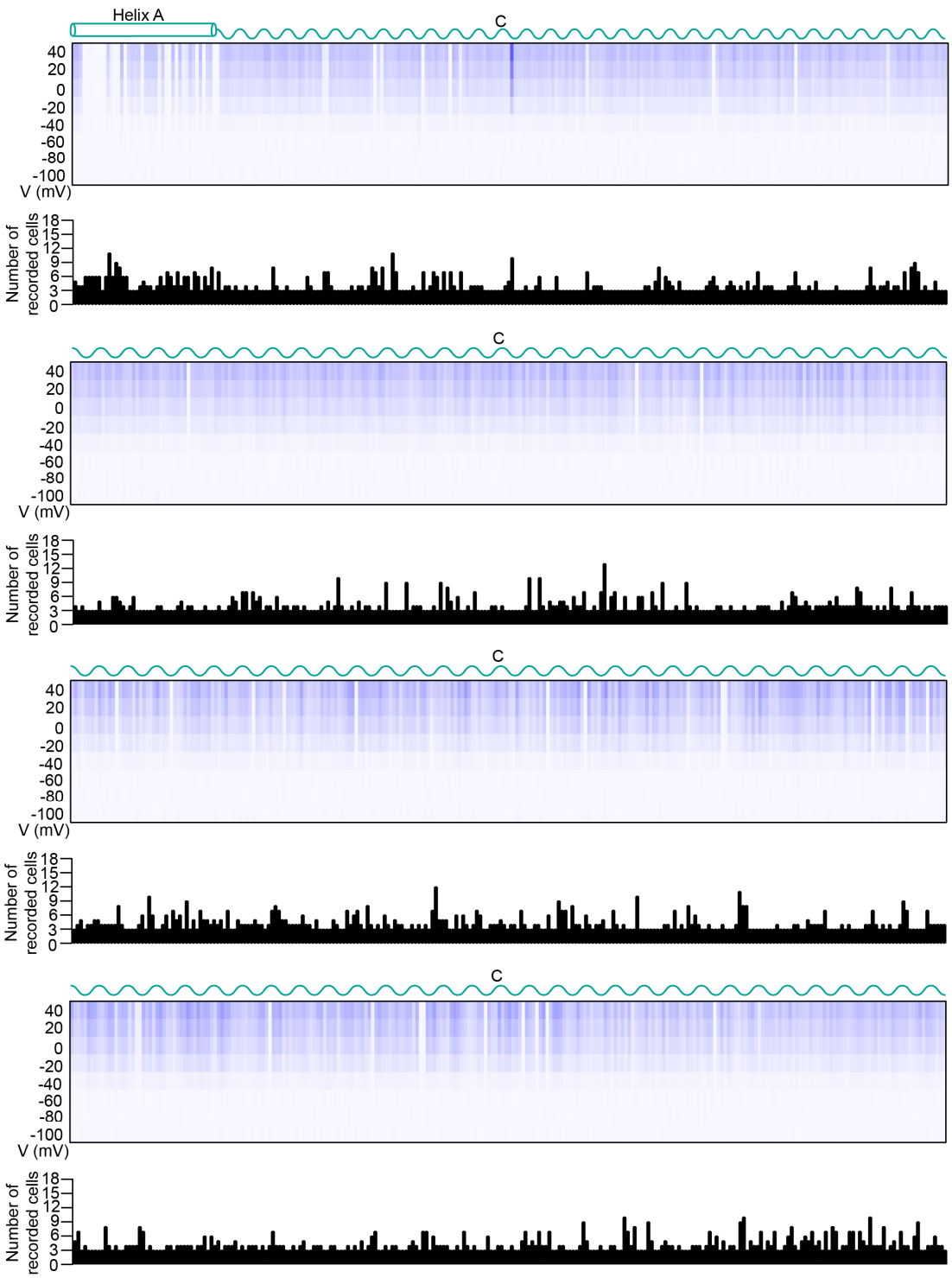
Helix A
C
40
20
0
-20
-40
-60
-80
-100
V (mV)
Number of recorded cells
18
15
12
9
6
3
0
C
40
20
0
-20
-40
-60
-80
-100
V (mV)
Number of recorded cells
18
15
12
9
6
3
0
C
40
20
0
-20
-40
-60
-80
-100
V (mV)
Number of recorded cells
18
15
12
9
6
3
0
C
40
20
0
-20
-40
-60
-80
-100
V (mV)
Number of recorded cells
18
15
12
9
6
3
0

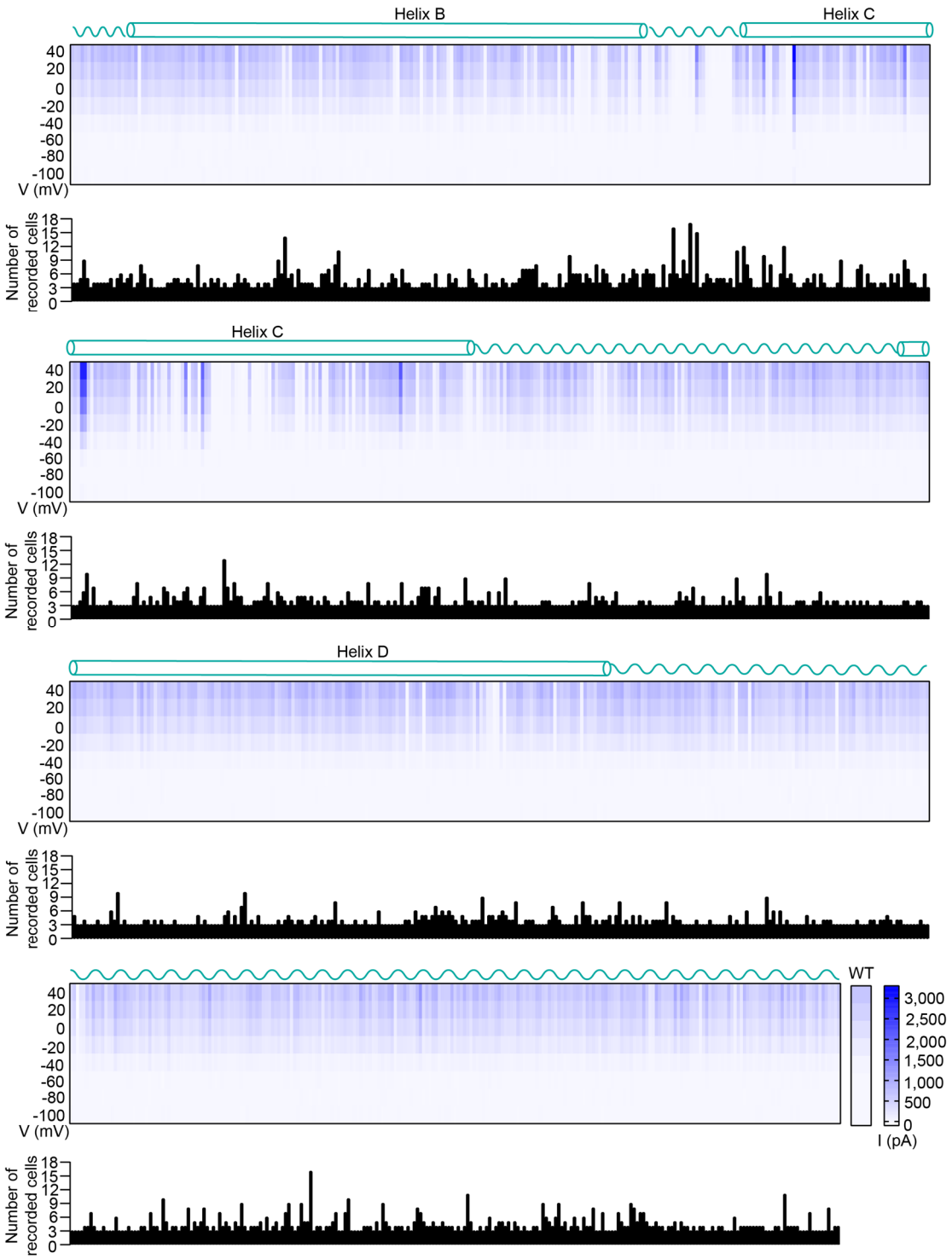

Supplemental Fig. S3: The mean current value of all 4,085 SNVs measured at a voltage of -100 mV to +40 mV when expressed alone. All 4,085 variants were ordered according to the amino acid position. There are 4-7 substitutions for each amino acid (except synonymous variants and nonsense variants). Different variants in the same

amino acid are arranged alphabetically. Each row contains 256 variants. The blue shade represents the current magnitude and the darker the color, the greater the current value. The wild-type currents were located at the end of all variants. The black histogram showed the number of recorded cells per variant. At least 3 cells were recorded for each variant. For variants with large variations in peak currents, the number of recorded cells would be increased. N-terminus: M1-G96; S1 transmembrane domain: W97-S119; S1-S2 linker: T120-H124; S2: Q125-C156; S2-S3 linker: C157-K172; S3: P173-G192; S3-S4 linker: T193-A199; S4: T200-M217; S4-S5 linker: D218-H234; S5: S235-A263; Pore region: N264-T293; S6: W294-F335; Helix A: K337-D356; Helix B: P528-L553; Helix C: K559-G588; Helix D: D611-G638.

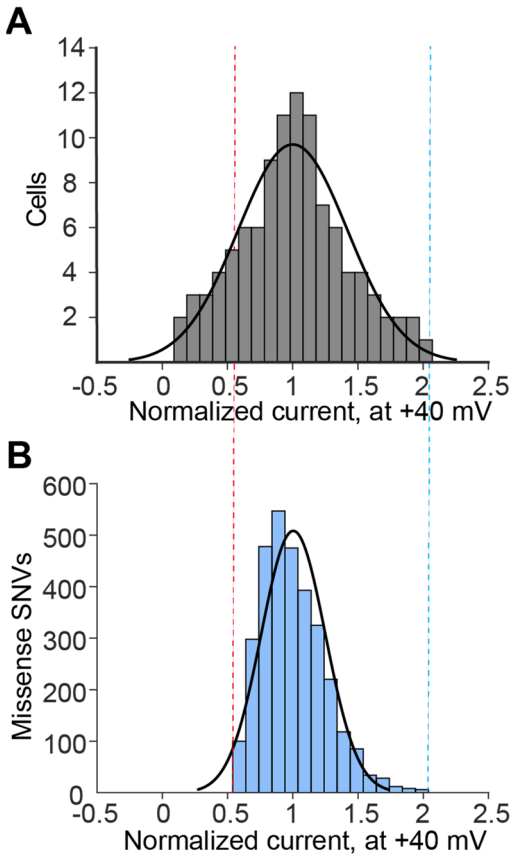

Supplemental Fig. S4: Comparison of the current distributions of wild-type KCNQ4 and 3,127 variants classified as 'normal current'. (A) The distribution of the normalized peak currents measured at +40 mV from 103 cells transfected with wild-type KCNQ4. (B) The peak current distribution for 3,127 *KCNQ4* missense SNVs classified as 'normal current' category in our functional classification based on the peak currents in the homozygous state.

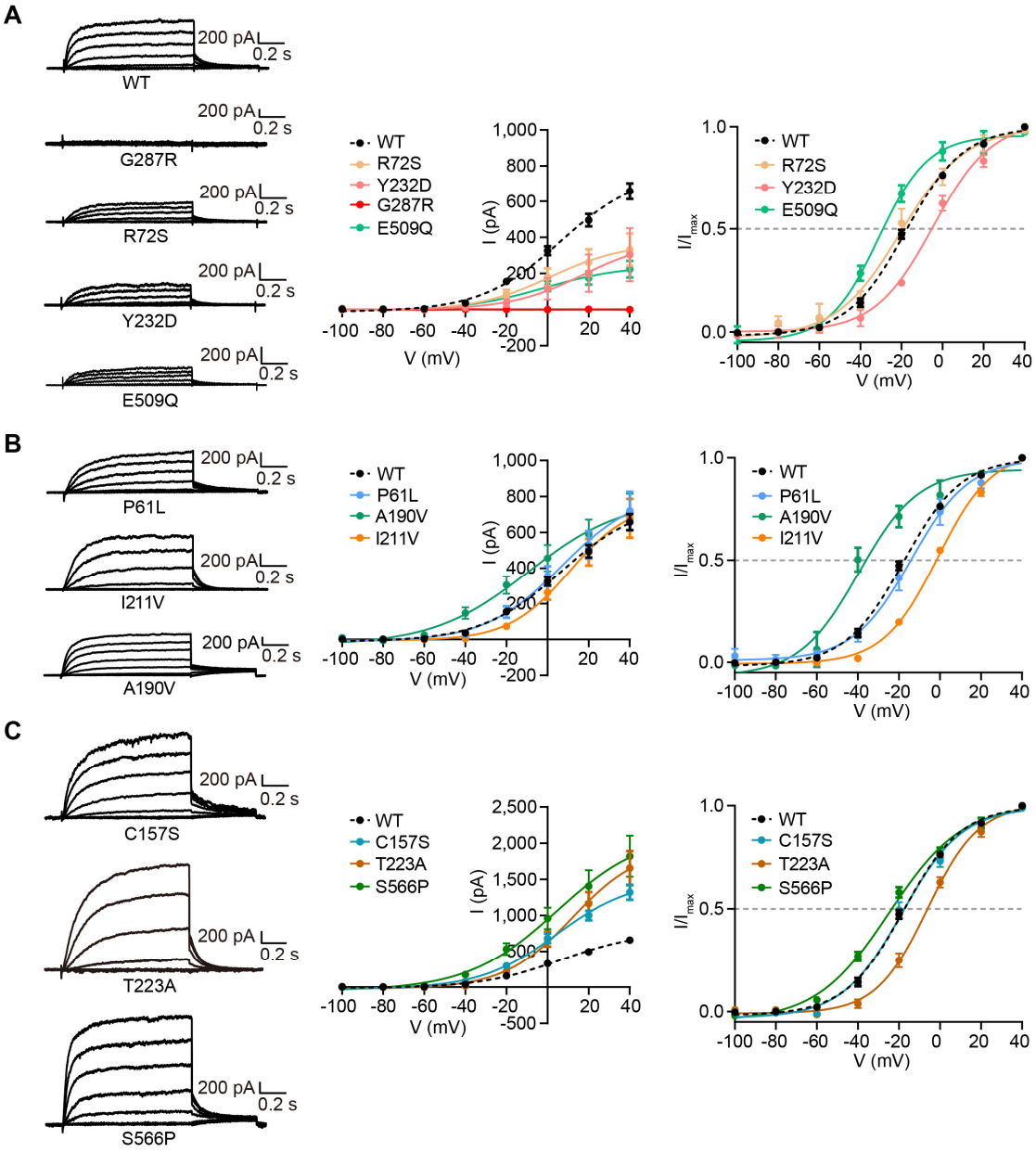

Supplemental Fig. S5: Representative functional properties of each type of variant.

(A) Representative current traces, mean current-voltage relation, and voltage dependence of steady-state activation curves generation from tail currents of variants classified as 'reduced current'. Voltage dependence of steady-state activation curves was generated by plotting the normalized tail current against membrane potentials using the Boltzmann function. (B) Representative current traces, mean current-voltage relation, and voltage dependence of steady-state activation curves of variants classified

as ‘normal current’. (C) Representative current traces, mean current-voltage relation, and voltage dependence of steady-state activation curves of variants classified as ‘enhanced current’.

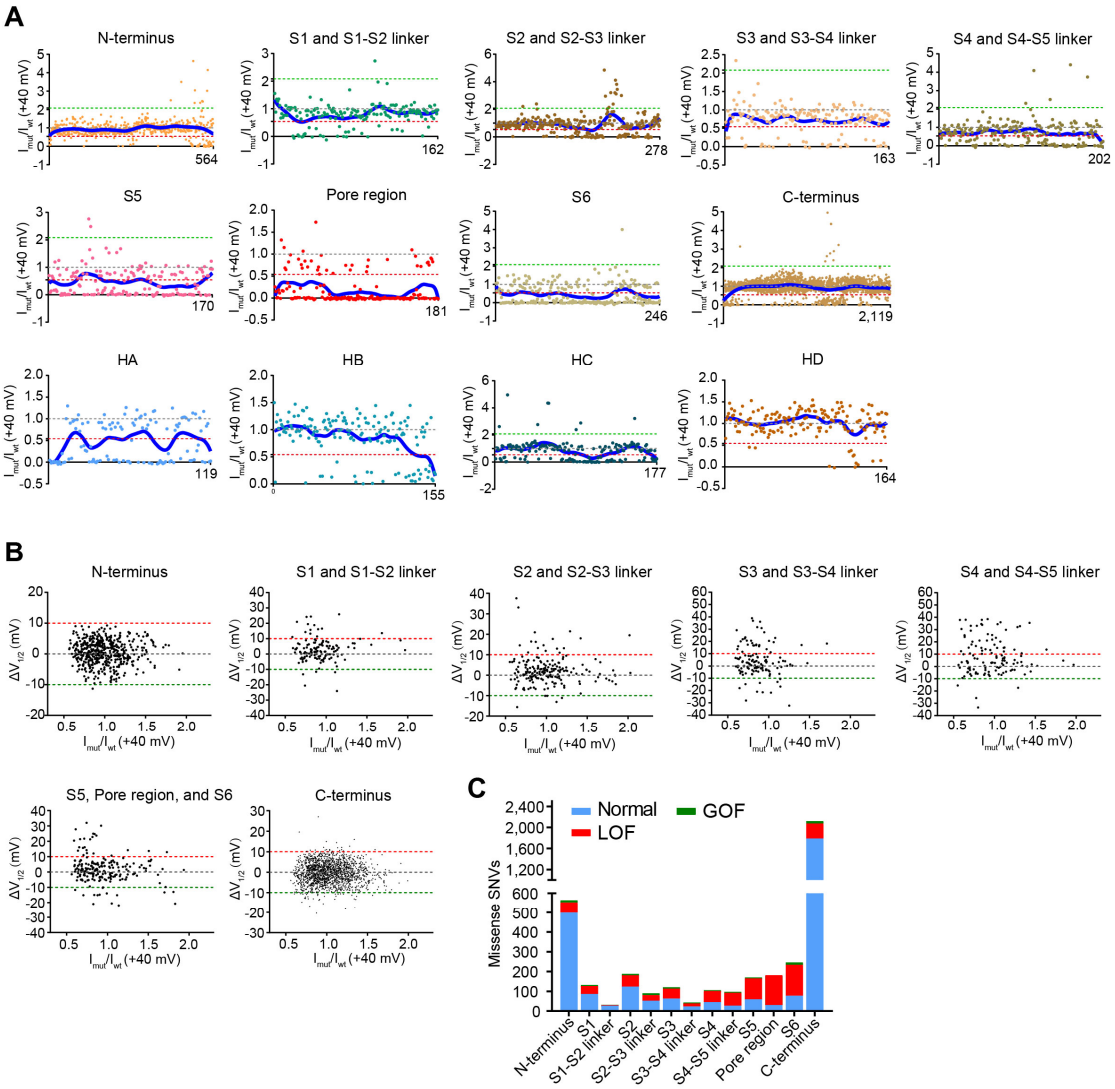

Supplemental Fig. S6: Normalized mean currents and $V_{1/2}$ distribution and functional classification of *KCNQ4* missense SNVs in each domain when expressed alone. (A) Plots shown here are the mean currents of all variants in each domain (averaged from n ≥ 3 cells). The number in the lower right corner of the X-axis of each graph indicates the variant number contained in the corresponding area. The red dotted line indicates 0.54 of the wild-type value, the grey indicates the wild-type, and the green represents 2.08 of the wild-type. All 4,085 variants are ordered by amino acid number. Different variants in the same amino acid are arranged alphabetically. Positional biases in current values were modeled for 4,085 missense SNVs by using a LOWESS

regression to fit the normalized currents recorded at +40 mV when transfected alone. (B) $V_{1/2}$ characteristic of 3,127 missense SNVs with normal currents in each domain when expressed alone. The red dotted line indicates 10 mV rightward shifts in $V_{1/2}$, the grey indicates the wild-type, and the green indicates 10 mV leftward shifts in $V_{1/2}$. (C) The number of missense SNVs in each domain was plotted and colored by functional classification.

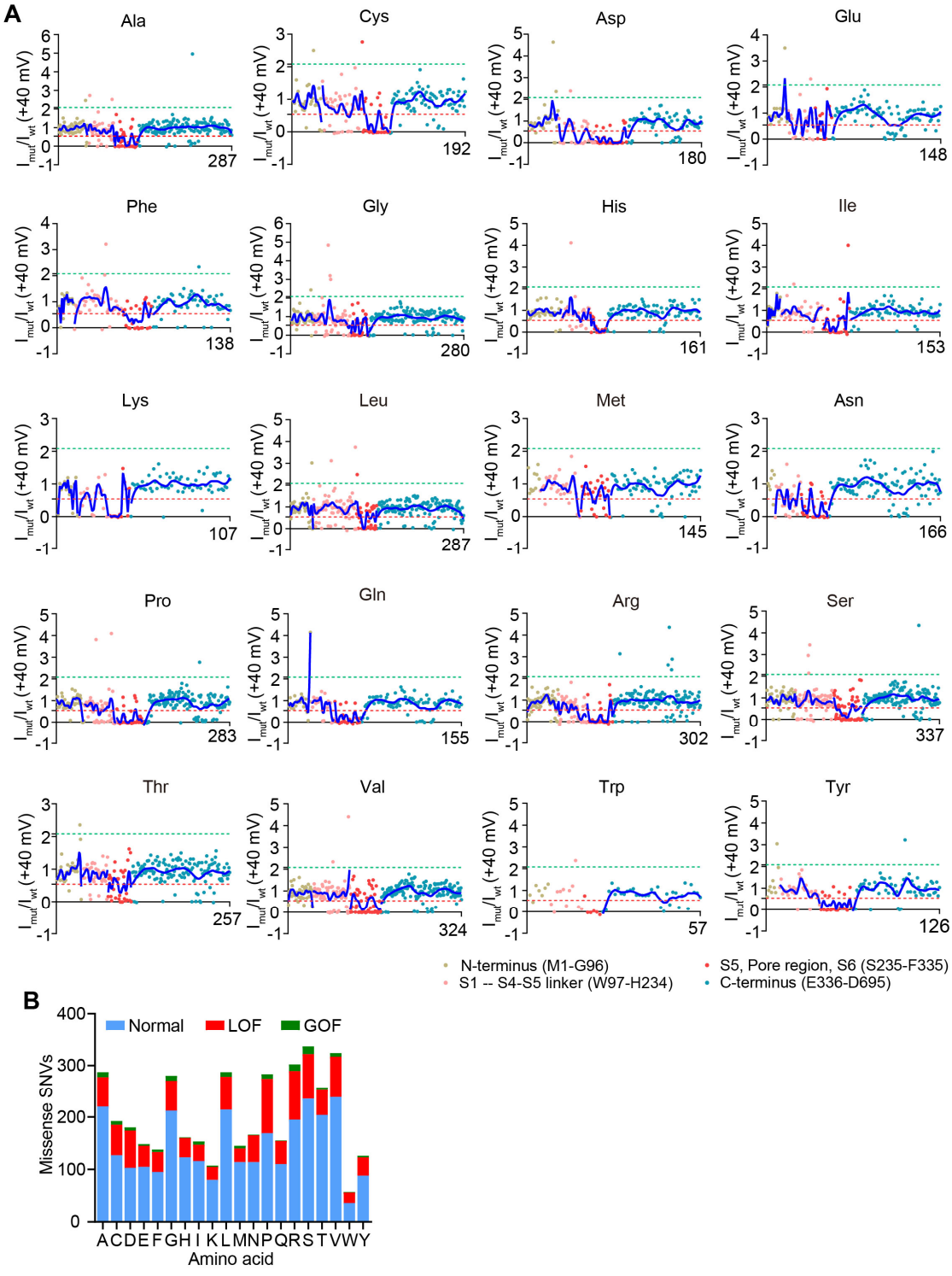

Supplemental Fig. S7: Normalized mean currents distribution and functional classification of each type of amino acid after mutation. (A) Plots shown here are the mean currents of all amino acids (averaged from n ≥ 3 cells). The number in the lower right corner of the X-axis of each graph indicates the variant number in the

corresponding amino acid. The red dotted line indicates 0.54 of the wild-type currents and the green represents 2.08 of the wild-type currents. Positional biases in current values were modeled for 4,085 missense SNVs by using a LOWESS regression to fit the normalized currents recorded at +40 mV when transfected alone. Each domain was fitted separately. Several missing fittings were due to the limited variants. (B) The number of missense SNVs of each type of amino acid was plotted and colored by functional classification. The number of variants per amino acid was Ala (A): 287; Cys (C): 192; Asp (D): 180; Glu (E): 148; Phe (F): 138; Gly (G): 280; His (H): 161; Ile (I): 153; Lys (K): 107; Leu (L): 287; Met (M): 145; Asn (N): 166; Pro (P): 283; Gln (Q): 155; Arg (R): 302; Ser (S): 337; Thr (T): 257; Val (V): 324; Trp (W): 57; Tyr (Y): 126.

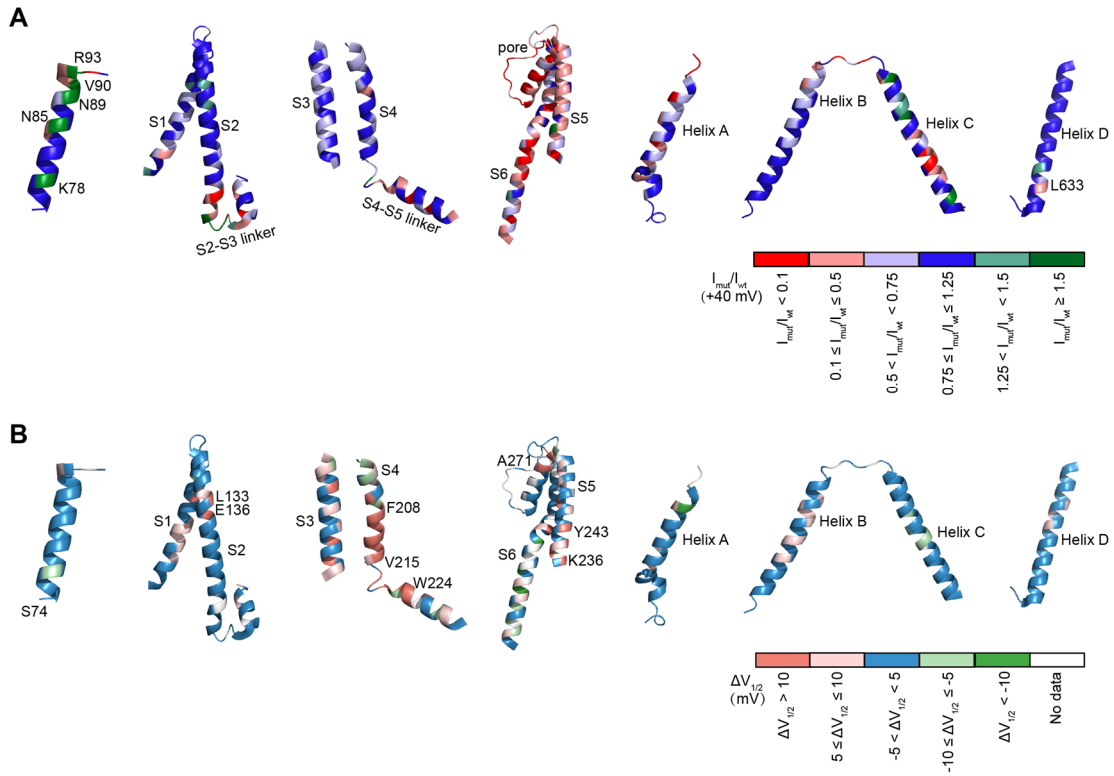

Supplemental Fig. S8: Details of structure basis for KCNQ4 channel. (A) Local cartoon diagrams show each domain of a KCNQ4 monomer. Colors indicate normalized current value averaging from 4-7 substitutions. Although helix D was not available in the KCNQ4 cryo-EM structure (PDB: 7BYL), its crystal structure has been resolved (PDB: 2OVC) (Howard et al. 2007). (B) Activation $V_{1/2}$ were mapped onto each domain of a KCNQ4 monomer. 13 of 164 variants in helix D exhibited reduced currents and only 4 of 157 variants with available $V_{1/2}$ in helix D had large shifts.

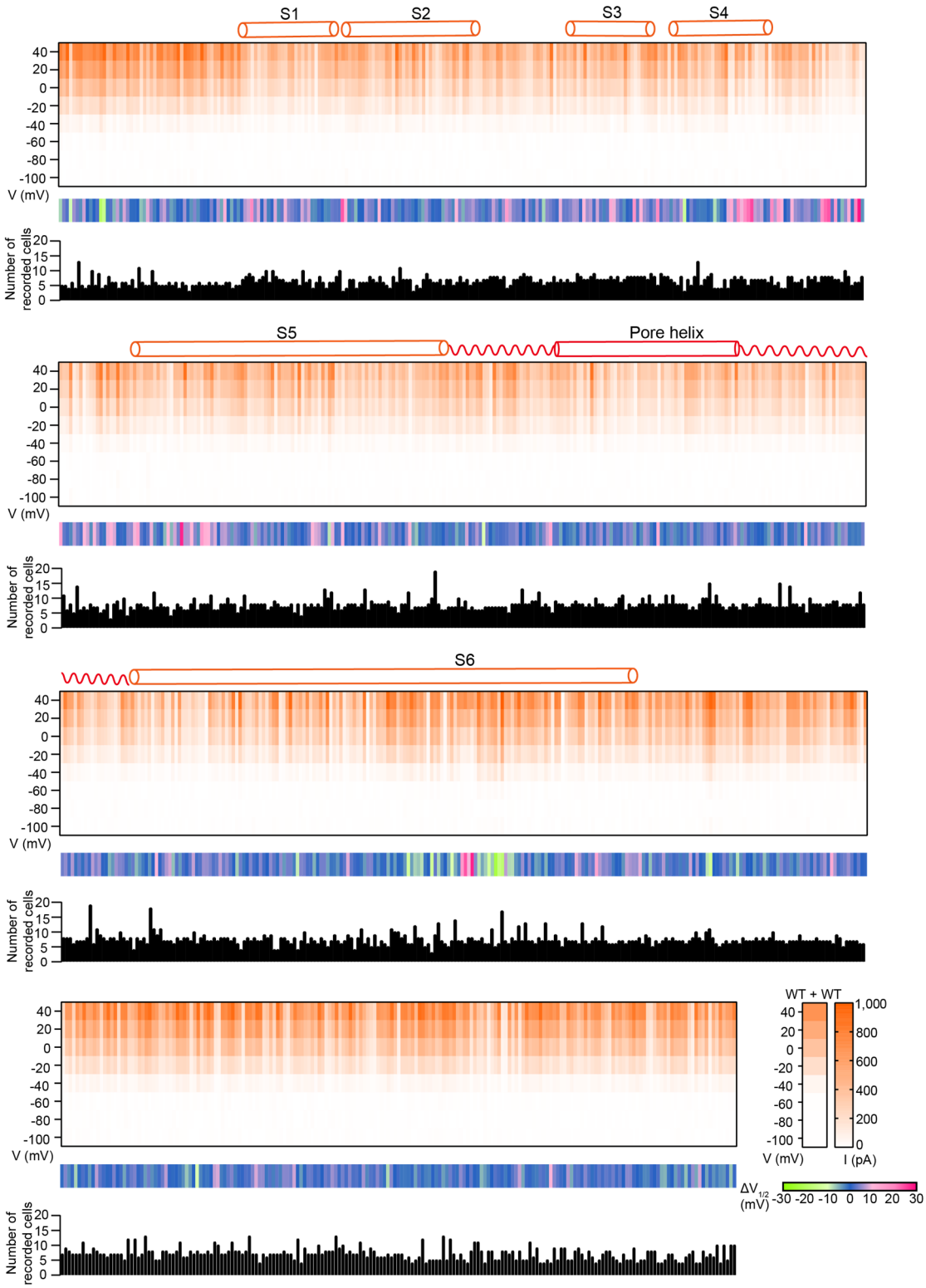

Supplemental Fig. S9: The mean current value of 915 variants with reduced currents when expressed alone measured at a voltage of -100 mV to +40 mV when co-expressed with wild-type. All 915 variants were ordered according to the amino

acid position. The wild-type currents (*KCNQ4*-Myc-EGFP + *KCNQ4*-Myc-mCherry) are located at the end of all 915 variants. The shifts of $V_{1/2}$ of 915 variants in the heterozygous state were shown with different indicated colors. The black histogram showed the number of recorded cells per variant. More than 5-6 cells were recorded for almost variants co-expressed with wild-type. For variants with large variations in peak currents, the number of recorded cells would be increased.

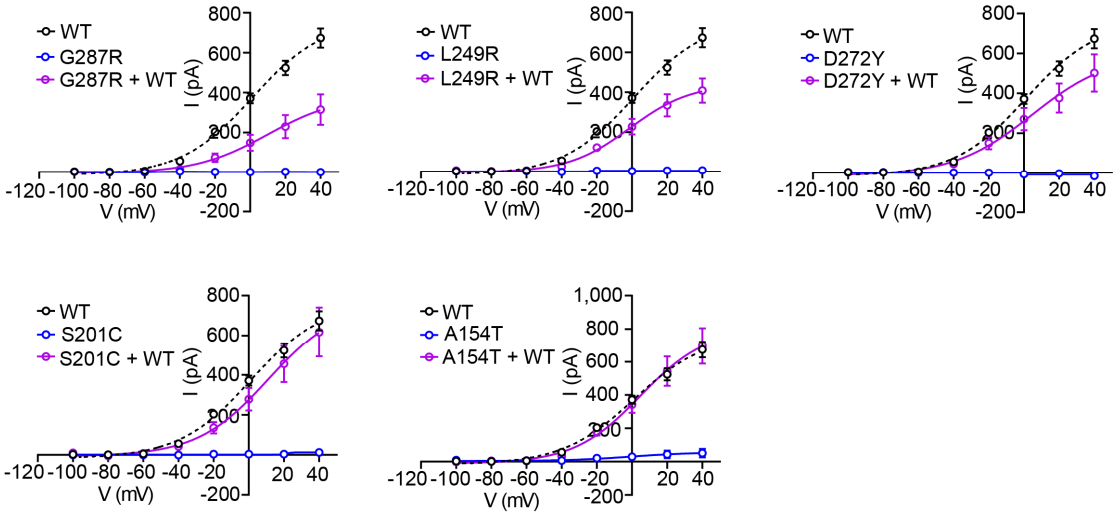

Supplemental Fig. S10: Electrophysiological recording results of five variants used to construct knock-in point mutation mice. Current-voltage relationships of wild-type KCNQ4 channels, variant KCNQ4 channels, and heterogeneous KCNQ4 channels (co-expression wild-type KCNQ4 channels and variants at a ratio of 1:1). ($n \geq 3$; mean ± SEM).

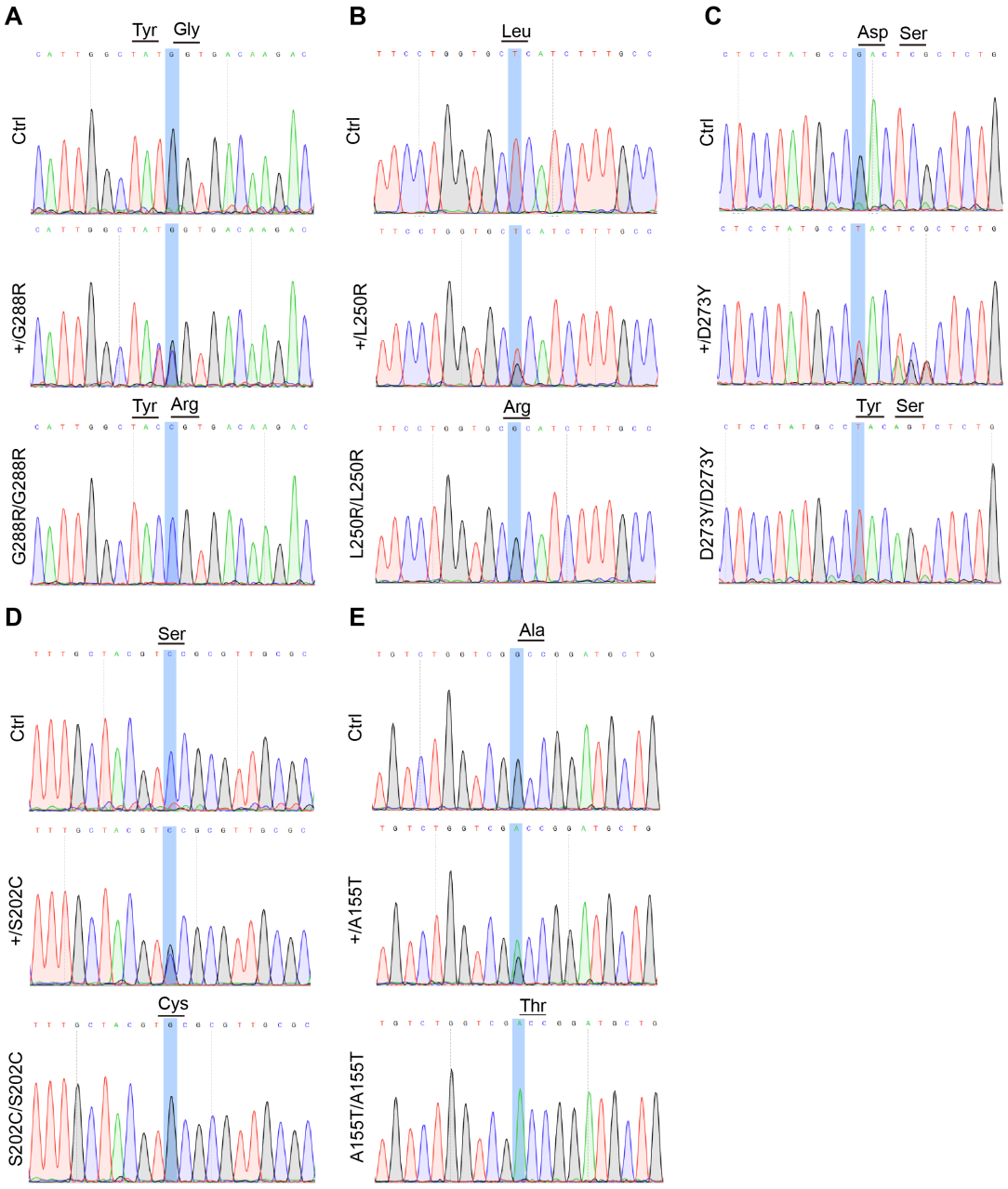

Supplemental Fig. S11: Genotype for point mutant mice. Mutations were validated by DNA Sanger sequencing in p.G288R, p.L250R, p.D273Y, p.S202C, and p.A155T mutant KI mice. Upper panels represent the wild-type alleles, middle panels are the heterozygote mutant mice, and lower panels are the homozygote mutant mice. Silent mutations (TAT to TAC in p.G288R mutant mice and TCG to AGT in p.D273Y mutant mice) were introduced to prevent the binding and recutting of the sequence by gRNA after homology-directed repair.

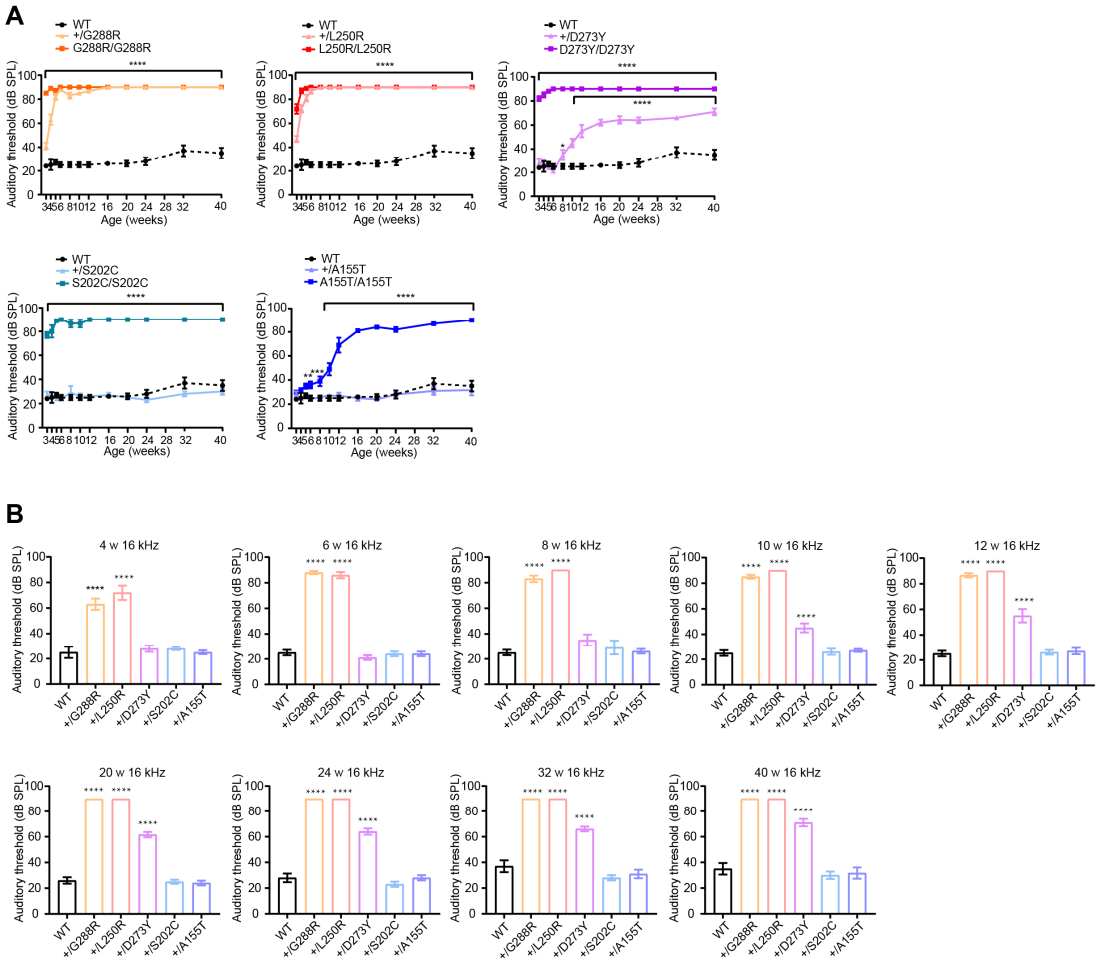

Supplemental Fig. S12: ABR measurement of wild-type, homozygous mutant, and heterozygous mutant mice at 16 kHz. (A) Auditory threshold for each mutant mouse strain at 16 kHz. Data were analyzed by two-way ANOVA with a Dunnett correction. ****$P < 0.0001$, ***$P < 0.001$, **$P < 0.01$, *$P < 0.05$. (B) Comparison of auditory threshold of wild-type and heterozygous mutant mice at 4, 6, 8, 10, 12, 20, 24, 32, and 40 weeks old of age at 16 kHz. Data are mean ± SEM. Statistical analysis was performed using one-way ANOVA with Dunnett's multiple comparisons. ****$P <$ 0.0001.

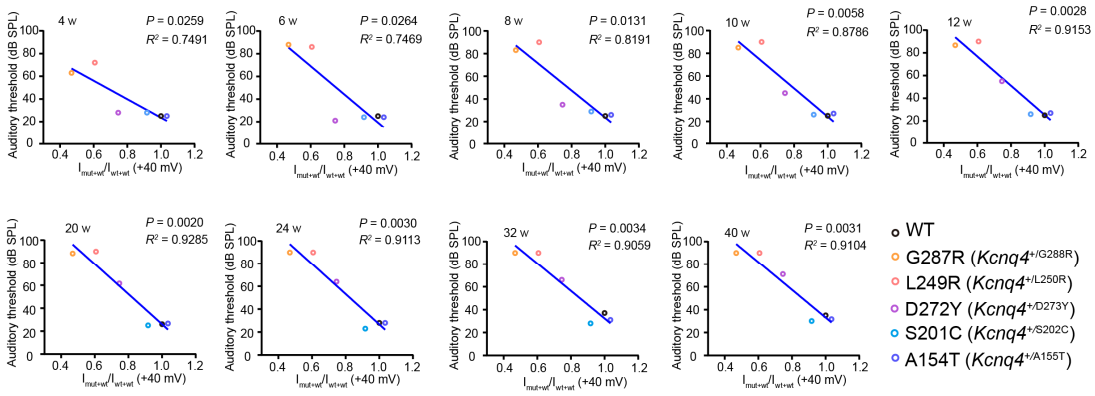

Supplemental Fig. S13: Correlational analysis between normalized peak currents measured from co-expressing five variants with wild-type channels and auditory threshold in wild-type and five *Kcnq4* mutant heterozygous mouse strains at 16 kHz. One point indicates one mutant. R^2 and P values were noted for each plot analyzed from Pearson's correlation.

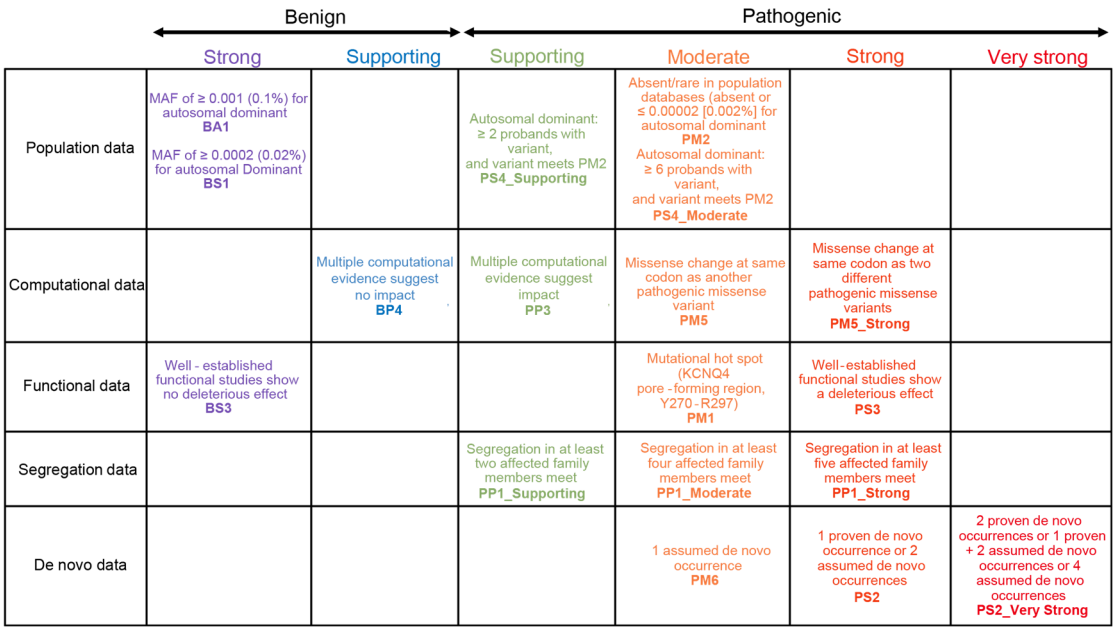

Supplemental Fig. S14: ACMG/AMP classification criteria used to classify the pathogenicity of *KCNQ4* missense variants.

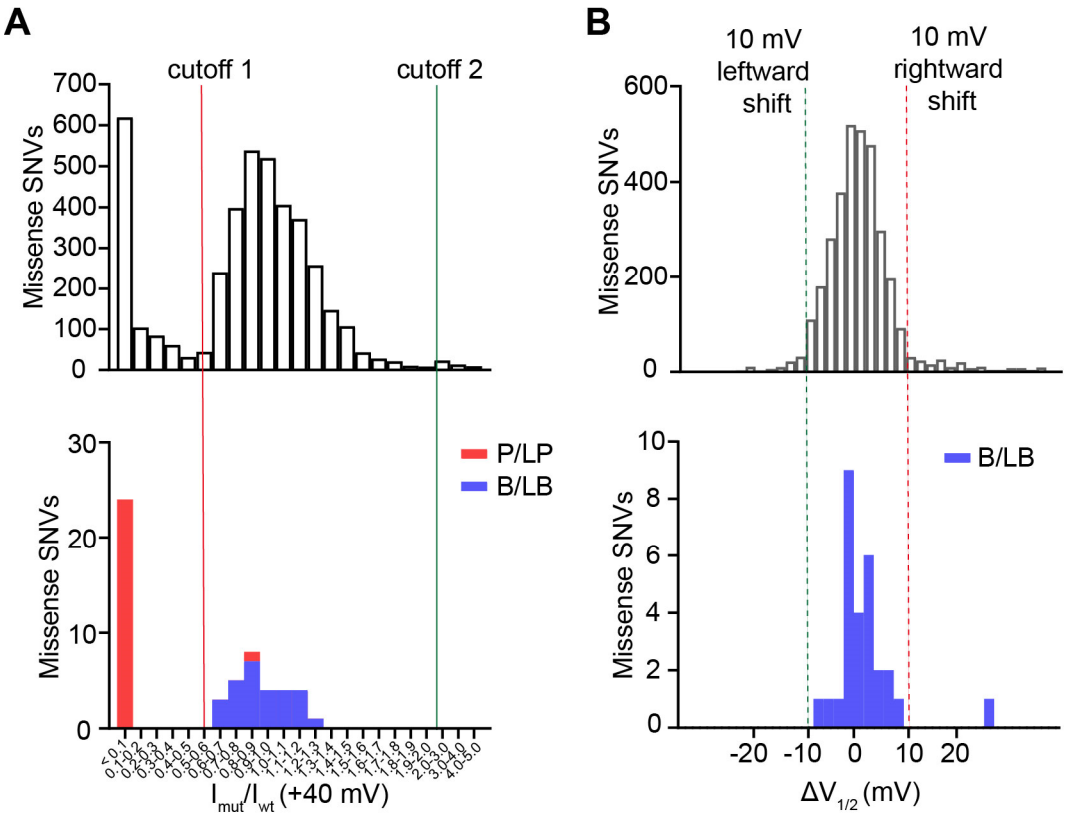

Supplemental Fig. S15: Functional properties of 25 known pathogenic/likely pathogenic and 28 known benign/likely benign variants when expressed alone. (A) The normalized peak currents distribution for all variants (upper) and 25 known pathogenic/likely pathogenic and 28 known benign/likely benign variants (lower) when expressed alone. 53 missense variants colored by pathogenicity classification were based on ACMG/AMP criteria without our patch-clamp data. The red line indicates the cutoff between reduced currents and normal currents and the green indicates the cutoff between normal currents and enhanced currents. (B) The distribution of the shifts in $V_{1/2}$ ($\Delta V_{1/2}$) for all variants (upper) and 28 benign/likely benign variants (lower) when expressed alone.

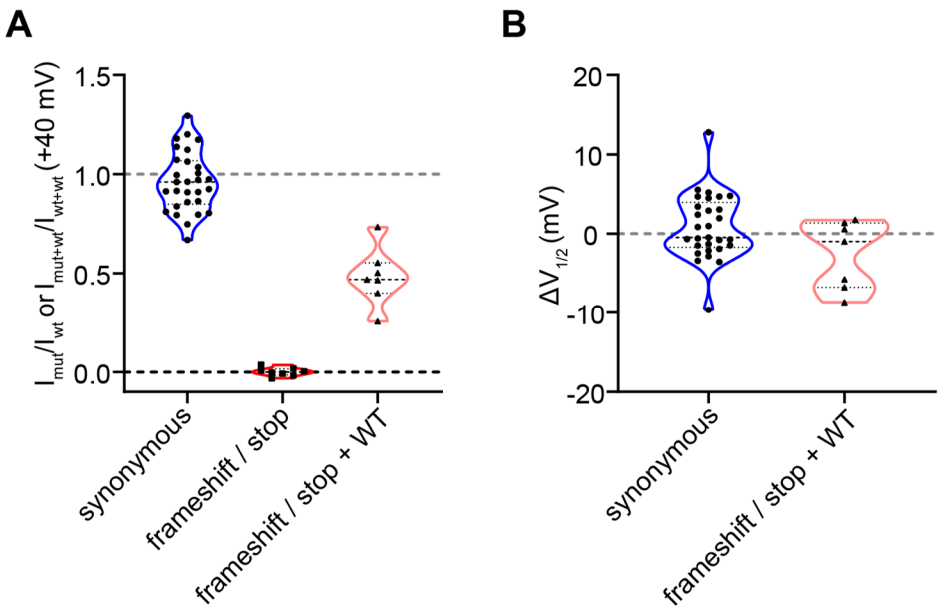

Supplemental Fig. S16: Functional properties of 29 synonymous variants, 6 frameshift variants and 1 stop-gained variant. 29 synonymous variants were collected from 1000 Genomes Project, and 6 frameshift variants and 1 stop-gained variant were reported in DFNA2 pedigrees.

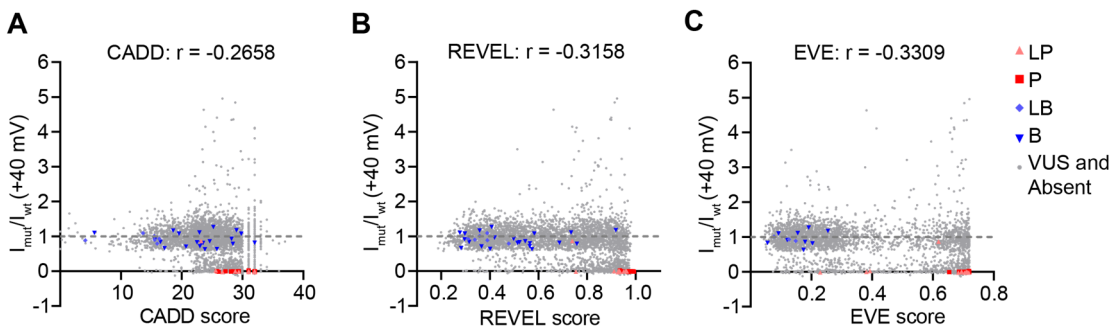

Supplemental Fig. S17: Computational predictions for pathogenicity. Correlations between computational predictors (CADD, REVEL, and EVE) with normalized peak currents. (Spearman's correlation, $P < 0.0001$ for all correlations). Variants are colored based on the ACMG pathogenicity interpretation without our patch clamp study. VUS and Absent: variants with uncertain significance and variants missing in databases.